

Cite this: *J. Mater. Chem. C*, 2019, 7, 558

A universal host material with a simple structure for monochrome and white phosphorescent/TADF OLEDs†

Chao Wu,^a Binyan Wang,^a Yafei Wang,^a ^b Jianyong Hu, ^a Jiaxing Jiang, ^{*a} Dongge Ma^c and Qiang Wang ^{*a}

The development of universal host materials suitable for both phosphorescent and thermally activated delayed fluorescent (TADF) emitters is still a bottleneck for fabricating highly efficient full-color and white organic light-emitting diodes (OLEDs) with a simple device structure. In this paper, two novel donor–acceptor type bipolar hybrids with simple molecular structures, 4'-(diphenylamino)-[1,1'-biphenyl]-4-carbonitrile (**TPA-BN**) and 4-(3-(4-(diphenylamino)phenyl)propyl)benzotrile (**TPA-L-BN**), were designed and synthesized by combining triphenylamine as the electron-donating unit with benzotrile as the electron-accepting unit. Their thermal, morphological, electrochemical, photophysical, charge transporting, and electroluminescent properties were comprehensively characterized for demonstrating their potential use as host materials for the fabrication of both phosphorescent and TADF OLEDs. The introduction of a flexible aliphatic spacer into **TPA-L-BN** gives rise to a high triplet energy of 2.95 eV due to the interruption of π -conjugation. The phosphorescent and TADF OLEDs based on the two hosts exhibit superior electroluminescence (EL) performance with high efficiencies and low roll-offs, employing a simplified and unified device structure. In particular, **TPA-L-BN** can host deep blue to red phosphorescent emitters and the blue TADF emitter with external quantum efficiencies over 20%. In addition, highly efficient all phosphorescent and TADF/phosphorescent hybrid white OLEDs (WOLEDs) with complementary emitters were realized using **TPA-L-BN** as the single host material. **TPA-L-BN** was also adopted to fabricate single-host three primary color WOLEDs, producing maximum efficiencies of 57.1 cd A⁻¹, 53.6 lm W⁻¹, and 23.4% with a high color rendering index of 83. The EL spectra of all these WOLEDs showed remarkable color stability with very small color variations across the whole range of luminance. More importantly, the **TPA-L-BN** hosted device presented a longer lifetime than that of the device based on **TPA-BN**, because of the improved morphological stability of **TPA-L-BN** in the emitting layer. These excellent results obtained using the non-conjugated bipolar hybrid host **TPA-L-BN** show that the introduction of the flexible linkage between the donor and the acceptor is an effective approach to construct universal host materials for highly efficient and stable phosphorescent and TADF OLEDs.

Received 18th October 2018,
Accepted 12th December 2018

DOI: 10.1039/c8tc05259j

rsc.li/materials-c

^a Key Laboratory of Applied Surface and Colloid Chemistry, National Ministry of Education, Shaanxi Key Laboratory for Advanced Energy Devices, Shaanxi Engineering Lab for Advanced Energy Technology, School of Materials Science and Engineering, Shaanxi Normal University, Xi'an 710119, P. R. China.
E-mail: qiangwang@snnu.edu.cn, jiaxing@snnu.edu.cn

^b Jiangsu Key Laboratory of Environmentally Friendly Polymeric Materials, School of Materials Science and Engineering, Jiangsu Collaboration Innovation Center of Photovoltaic Science and Engineering, Changzhou University, Changzhou 213164, P. R. China

^c Institute of Polymer Optoelectronic Materials and Devices, State Key Laboratory of Luminescent Materials and Devices, South China University of Technology, Guangzhou 510640, P. R. China

† Electronic supplementary information (ESI) available: Experimental details including the synthetic procedures, PL spectra and quantum yields of **TPA-BN** and **TPA-L-BN** films doped with blue, green, and red emitters; calculated spatial distributions of the HOMO and LUMO levels; the EL performance of the green, orange, and red PhOLEDs based on **TPA-L-BN**; NMR spectra; and MS spectra. See DOI: 10.1039/c8tc05259j

Introduction

Organic light-emitting diodes (OLEDs) have progressed rapidly in terms of both materials and device techniques in academic and commercial fields over the past few decades, due to their advantages such as high efficiency, ultra-thinness, lightness and flexibility for applications in flat panel display and solid-state lighting.^{1–4} By harvesting all the electrically generated singlet and triplet excitons for 100% theoretical internal quantum efficiency (IQE), phosphorescent OLEDs (PhOLEDs)⁵ and thermally activated delayed fluorescence (TADF) diodes⁶ have drawn considerable attention in the fields of practical applications and science. These two diodes can make all the excitons converge to radiative excited states of the phosphorescent and TADF emitters,

namely the first triplet (T_1) and singlet (S_1) excited states, through intersystem crossing (ISC) and reverse ISC (RISC), respectively. To minimize energy loss due to collision-induced quenching caused by the long emission lifetime of phosphors and TADF emitters, both PhOLEDs and TADF diodes are usually fabricated with a host-guest doping structure in the emitting layer by adopting host materials with sufficiently high triplet energies (E_T s). As an ideal candidate for future solid-state lighting sources, white OLEDs (WOLEDs) have drawn great attention from both academic research groups and commercial companies.^{7–10} WOLEDs with a single-host emitting layer (EML) have shown superior electroluminescence (EL) performance due to reduced structural heterogeneity and smooth charge injection and transport between different emissive centers.^{11–14} Since the relatively unstable blue phosphors restrict the development of all-phosphorescence WOLEDs in future massive production, hybrid WOLEDs, combining stable blue fluorescent dyes and efficient long-wavelength complementary color phosphors, are considered as an alternative for realizing high efficiency and long-life WOLEDs.^{14–22} However the efficiency of hybrid WOLEDs with conventional fluorescent materials is still far behind the expected values. Recently, hybrid WOLEDs based on highly efficient blue TADF emitters have provided an alternative for achieving white EL emission with comparable device efficiency to that of all phosphorescent WOLEDs.^{23–27} In order to reduce interfaces and eliminate the injection barrier between different EMLs, it is essential to employ only one host material for both TADF and phosphorescent emitters, which requires the development of universal host materials with high E_T values.^{28–30} As one of the earliest groups developing new host materials for both TADF and phosphorescent emitters, we synthesized a series of high performance host materials which were used to achieve both highly efficient TADF and PhOLED devices. A representative molecule, 9,9'-(2'-(1*H*-benzimidazol-1-yl)-[1,1'-biphenyl]-3,5-diyl)-bis(9*H*-carbazole) (*o*-mCPBI), synthesized by integrating 1,3-bis-(carbazol-9-yl)benzene (mCP) with a benzimidazole moiety *via* the *ortho*-position of *N*-phenyl, exhibited an extremely high E_T value of 3.00 eV.³¹ Blue, green, yellow, red, and white PhOLEDs with external quantum efficiencies (EQEs) of 20% or higher have been achieved by using *o*-mCPBI as the host. Single-host white OLEDs exhibited impressive color stability and a superior color rendering index. TADF OLEDs hosted by *o*-mCPBI achieved comparable or higher efficiencies in comparison with the reported values. Bonding electron-donating (donor, D) and electron-accepting (acceptor, A) moieties chemically into a single bipolar molecule is a common design strategy to achieve high and balanced electric flux, which prevents the accumulation of charges and excitons at interfaces. The capability of the D–A type bipolar hybrid hosts has been demonstrated for facilitating injection and transport of holes and electrons, broadening the recombination zone, and consequentially alleviating the efficiency roll-off.^{32–36} To further enhance the stability of the OLEDs, it is essential to avoid crystallization which may lead to charge trapping and luminance quenching.^{37–39} Bipolar hybrid compounds with flexible linkages have been demonstrated to possess superior morphological stability against crystallization and electronically decoupled donor and

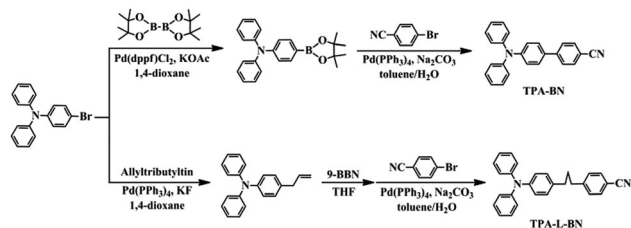
acceptor moieties retaining their individual functionalities, such as E_T and frontier molecular orbital levels.^{40–44} In addition, the PhOLEDs using non-conjugated hosts show improved device lifetime in comparison with the devices based on hosts consisting of directly linked donor and acceptor moieties.⁴³ Therefore, bipolar hybrid compounds with flexible linkages could be an ideal candidate for high performance materials hosting both TADF and phosphorescent emitters.

In this work, a universal host material with a simple structure was designed and synthesized by connecting triphenylamine (TPA) as the donor moiety and benzonitrile as the acceptor moiety through a non-conjugated propylene spacer. Compared to extensively used carbazole derivatives, TPA also has a high E_T value and good hole-transporting ability, but a shallower HOMO level being close to that of the widely used hole transporting materials, thus allowing efficient hole injection.^{44–47} The cyano group is an excellent acceptor for TADF emitters featuring advanced photoluminescence properties due to its strong electron-withdrawing ability and structural simplicity.^{6,48–51} Using the same donor and acceptor moieties, another new host material without the flexible spacer was also prepared for comparison. The new host material with the flexible spacer, 4-(3-(4-(diphenylamino)phenyl)propyl)benzonitrile (**TPA-L-BN**), exhibited a high E_T value of 2.95 eV, compared to 2.44 eV of the host with directly linked donor and acceptor moieties, namely 4'-(diphenylamino)-[1,1'-biphenyl]-4-carbonitrile (**TPA-BN**). By employing a simple and unified device structure, both phosphorescent and TADF OLEDs showed excellent performance using **TPA-L-BN** as the host. In addition to monochrome OLEDs, single-host complementary and three primary color WOLEDs with EQEs of over 20% and stable white color emission were also achieved, including hybrid WOLEDs with blue TADF materials. Furthermore, the operational stability of the **TPA-L-BN** based device is substantially raised compared to that of the **TPA-BN** based device. These performances of the non-conjugated bipolar host **TPA-L-BN** make it a universal host material for both highly efficient phosphorescent and TADF OLEDs.

Results and discussion

Synthesis and characterization

The chemical structures and synthetic routes to 4'-(diphenylamino)-[1,1'-biphenyl]-4-carbonitrile (**TPA-BN**) and 4-(3-(4-(diphenylamino)phenyl)propyl)benzonitrile (**TPA-L-BN**) are depicted in Scheme 1. It can be seen that the molecular structures of both compounds were very simple and their synthetic procedures were relatively easy. The starting compound 4-bromo-*N,N*-diphenylaniline was synthesized from diphenylamine and 1,4-dibromobenzene following the literature procedure.⁴¹ Both final compounds were prepared using palladium-catalyzed Suzuki coupling reactions. All reactions were carried out under nitrogen and anhydrous conditions unless noted otherwise. All these new compounds were purified by column chromatography on silica gel using ethyl acetate/petroleum ether as the eluent and obtained with high yields. The chemical structures



Scheme 1 Synthesis of TPA-BN and TPA-L-BN.

of the two final compounds were confirmed by ^1H and ^{13}C NMR spectroscopy, mass spectrometry, and elemental analysis (see further details of the synthesis in the ESI†).

Thermal properties

The thermal and morphological stabilities of the new host materials were investigated by thermogravimetric analysis (TGA) and differential scanning calorimetry (DSC) measurements. The thermal decomposition (T_d , corresponding to 5% weight loss) and glass transition temperature (T_g , according to the second heating scan) values recorded at a scanning rate of $10\text{ }^\circ\text{C min}^{-1}$ under a nitrogen atmosphere are shown in Fig. 1 and Table 1. As shown in Fig. 1, the two new compounds are thermally stable with T_d values of 317 and $305\text{ }^\circ\text{C}$ for TPA-BN and TPA-L-BN, respectively, which are desirable for host materials as they can bear high

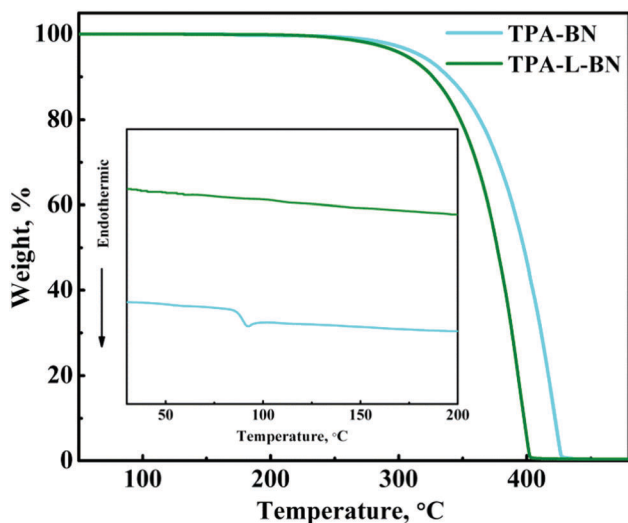


Fig. 1 TGA and DSC (inset) traces of TPA-BN and TPA-L-BN recorded at a heating rate of $10\text{ }^\circ\text{C min}^{-1}$.

temperatures during materials evaporation and device operation. According to the second heating scan using DSC, the T_g value of TPA-BN reached up to $90\text{ }^\circ\text{C}$ while the heating scan of TPA-L-BN showed no clear endothermic peak related to the glass transition (the inset of Fig. 1).

Photophysical properties

The UV-vis absorption and photoluminescence (PL) spectra in dilute solutions and thin solid films of the new hosts, as well as their phosphorescence spectra in toluene at 77 K, are presented in Fig. 2 and the corresponding data are summarized in Table 1. The absorption bands around 300 nm for both compounds could be assigned to triphenylamine-centered $n-\pi^*$ transition.⁵² The longer wavelength band at 360 nm of TPA-BN could be attributed to the $\pi-\pi^*$ transition from the triphenylamine moiety to the benzonitrile moiety, indicating that the photo-induced intramolecular charge transfer (ICT) state formation was made possible by some degree of π -conjugation through the biphenyl core.^{53,54} Because of the totally broken conjugation by the aliphatic spacer, no clear absorption due to $\pi-\pi^*$ transitions from the triphenylamine moiety to the benzonitrile moiety was observed in the absorption spectrum of TPA-L-BN. The inhibition of ICT also allows TPA-L-BN to present PL peaks at shorter wavelengths than those of TPA-BN,

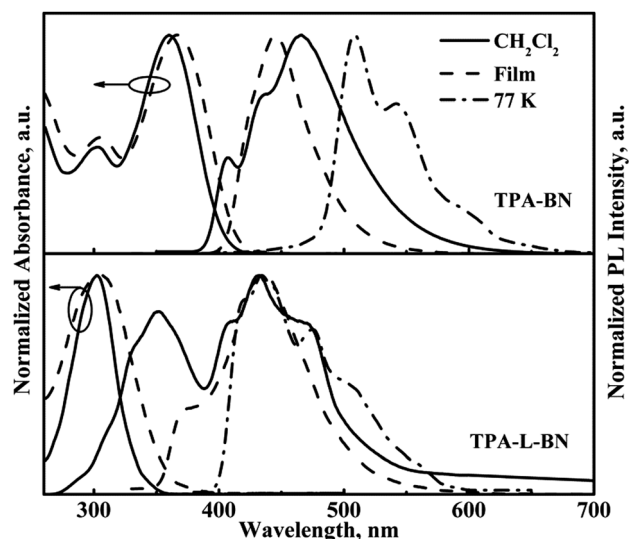


Fig. 2 UV-vis absorption, fluorescence spectra in dichloromethane and thin film state at room temperature, and the phosphorescence spectra in toluene at 77 K of TPA-BN and TPA-L-BN.

Table 1 The thermal, electrochemical and photophysical properties of TPA-BN and TPA-L-BN

Compound	T_d^a/T_g^b ($^\circ\text{C}$)	$\lambda_{\text{max,abs}}^d$ (nm)	$\lambda_{\text{max,em}}^d$ (nm)	$\lambda_{\text{max,abs}}^e$ (nm)	$\lambda_{\text{max,em}}^e$ (nm)	E_g^f (eV)	E_T^g (eV)	Φ_{PL}^h	HOMO/LUMO ⁱ (eV)
TPA-BN	317/90	360	407, 466	366	445	3.05	2.44	0.53	-5.36/-2.30
TPA-L-BN	305/— ^c	302	351, 433	306	437	3.65	2.95	0.20	-5.26/-1.89

^a Decomposition temperature (5% weight loss) obtained by TGA under N_2 . ^b Glass transition temperature obtained by DSC under N_2 . ^c Not available. ^d Absorption and emission peaks measured in dilute dichloromethane solution. ^e Absorption and emission peaks measured in thin solid films on quartz. ^f Optical band gap estimated from the absorption edge in dilute solution. ^g Triplet energy estimated from the phosphorescence spectra in toluene at 77 K. ^h Absolute fluorescence quantum yield obtained in the thin solid film using the calibrated integrating sphere system. ⁱ Calculated from the oxidation and reduction potentials of the compounds measured by cyclic voltammetry.

as shown in Fig. 2. The absorption spectra in the thin film state are almost similar to the absorption spectra in dilute solution, except for a slight red shift due to intermolecular interactions such as π - π stacking in the solid state.⁵⁵ It can be seen in Fig. 2 that both compounds show more structureless bands in the solid films with respect to those in solution. The possible reason for this could be that the molecules are excited to a locally excited state which then relax at an intermolecular charge transfer state because of tighter molecular packing or aggregation in neat solid films than in dilute solution.^{41,55} The quantum yields (Φ_{PL}) of neat films **TPA-BN** and **TPA-L-BN** were determined in an integrating sphere to be 0.53 and 0.20, respectively. The higher quantum yield of the **TPA-BN** film originates from the efficient radiative decay of the excited ICT state.⁴¹

To evaluate the prospects of the two compounds as hosts in OLEDs, the E_{T} values were determined using phosphorescence spectroscopy in toluene at 77 K. As shown in Fig. 2, the E_{T} values were estimated to be 2.44 and 2.95 eV for **TPA-BN** and **TPA-L-BN**, respectively, by taking the highest energy peak of phosphorescence as the transition energy of the triplet excited state to the ground state. The absence of π -conjugation through the biphenyl core enables **TPA-L-BN** to maintain a high E_{T} value which is adequate for hosting deep blue emitters. The relatively low E_{T} value of **TPA-BN**, which is attributed to the conjugation between the two moieties, makes it suitable only for green and red emitters. In order to further investigate energy transfer between the new hosts and widely used emitters, thin solid films of the two host materials doped with various phosphorescent emitters were prepared. From the fluorescence spectra of these films shown in Fig. S1 (ESI[†]), it can be seen that there is no observed emission from host materials, suggesting complete energy transfer from the host to the guest. This efficient energy transfer is confirmed by the high Φ_{PL} values of these films (Table S1, ESI[†]). Therefore, both **TPA-BN** and **TPA-L-BN** can be good host materials for both phosphorescent and TADF OLEDs. In particular, the universality of **TPA-L-BN** from deep blue to red emitters could be used to fabricate high performance WOLEDs.

Electrochemical and charge transporting properties

The electrochemical properties of the two hosts have been characterized by cyclic voltammetry (CV) in a 0.1 M solution of TBAPF₆ under a N₂ atmosphere. As shown in Fig. 3, the compounds undergo both reversible oxidation and reduction to permit the formation of stable cation and anion radicals, which implies their bipolar transporting properties. Their highest occupied molecular orbital (HOMO) and lowest unoccupied molecular orbital (LUMO) energy levels were calculated with reference to the energy level of ferrocene (4.80 eV below the vacuum level)⁵⁶ and are summarized in Table 1. Previous reports on non-conjugated bipolar hybrid compounds have demonstrated that the HOMO and LUMO levels of these compounds were essentially imported from those of the hole- and electron-transporting moieties as independent chemical entities, making it convenient to predict the energy levels of a given molecule before proceeding to synthesize it.^{40–44} The calculated HOMO level at -5.26 eV for **TPA-L-BN**, which is

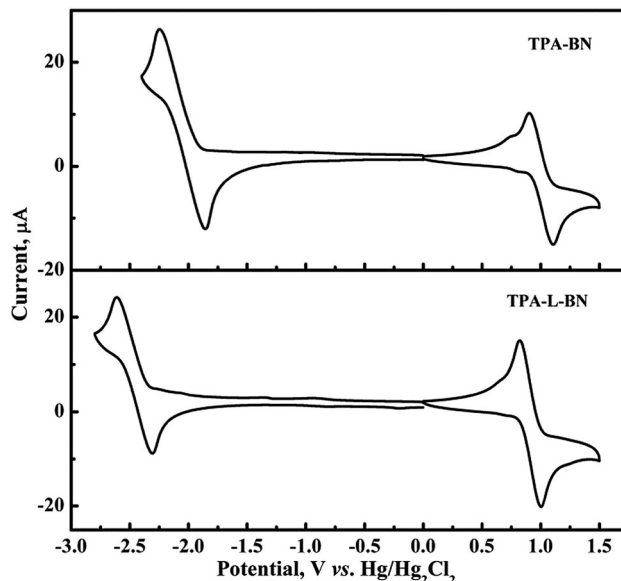


Fig. 3 CV scans of **TPA-BN** and **TPA-L-BN**.

almost identical to that of independent triphenylamine,⁴¹ confirms the above-mentioned statement. The HOMO levels of both compounds are a little higher than that of the widely used hole-transport material TAPC (-5.49 eV),⁵⁷ thus, the relatively easier transfer of holes and the resultant lower turn-on voltages are anticipated. The LUMO level of **TPA-L-BN** is estimated to be -1.89 eV, much smaller than -2.30 eV of **TPA-BN**. It is noteworthy that the electrochemical band gap of **TPA-BN** is 3.06 eV, which is very close to its optical band gap of 3.05 eV (Table 1), indicating that the 360 nm absorption peak represents the electronic transition from the HOMO level to the LUMO level. This electronic transition, however, is absent in **TPA-L-BN** where the ICT process is largely weakened.

To get deep insight into the electronic features of these two molecules, the geometrical and electronic properties of the compounds were studied using density functional theory (DFT) calculations. Fig. S2 (ESI[†]) shows the spatial distributions of the frontier molecular orbitals, calculated using the Gaussian 09 software package under the B3LYP/6-31G(d) basis set. For both molecules, the electron clouds of the HOMOs are situated on the TPA unit while the LUMOs are mainly localized on the benzonitrile segment. It is noted that **TPA-L-BN** shows complete separation of HOMO and LUMO electron distributions due to the broken conjugation between the electron-donating and electron-withdrawing moieties by the flexible spacer, which is consistent with the independent HOMO/LUMO levels by CV. Both the CV measurements and the DFT calculations imply the bipolar charge carrier transporting nature of the two D-A type compounds. To confirm this, the hole and electron transporting properties of the hosts were investigated by using hole-only and electron-only devices with configuration of ITO (indium tin oxide)/MoO₃ (5 nm)/TAPC (30 nm)/host (30 nm)/TAPC (30 nm)/Al (100 nm) and ITO/TmPyPB (30 nm)/host (30 nm)/TmPyPB (30 nm)/LiF (1 nm)/Al (100 nm). The current density versus voltage curves of the devices are shown in Fig. 4. Obviously, all

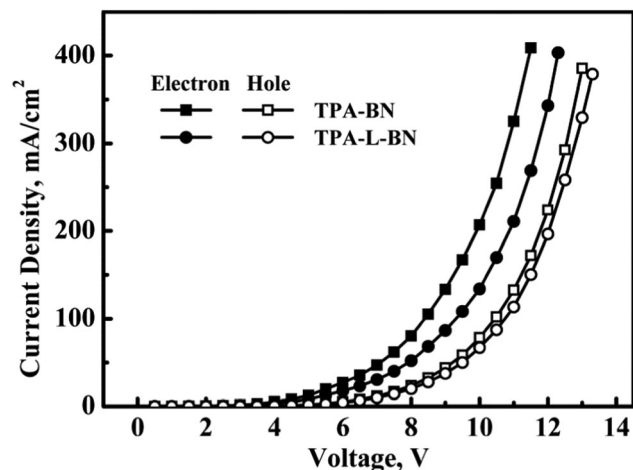


Fig. 4 Current density versus voltage characteristics of the hole-only and electron-only devices.

these unipolar devices can afford significant hole or electron currents, demonstrating their bipolar transporting nature. As a host, the bipolar character is preferable for balancing holes and electrons and broadening the recombination zone of the EML to alleviate the efficiency roll-off. It also can be seen that at the same voltage, both the hole and electron currents of devices based on **TPA-L-BN** are slightly lower than those of devices based on **TPA-BN**, largely due to the difference in molecular packing of the two molecules when forming thin films.⁴²

Electroluminescent properties

Inspired by the high thermal stabilities, suitable energy levels, bipolar charge transporting capabilities, and excellent photo-physical properties, especially the extremely high E_T of **TPA-L-BN**, both the compounds were further evaluated as the host in both phosphorescent and TADF OLEDs using the device configuration of ITO/MoO₃ (5 nm)/TAPC (60 nm)/mCP (10 nm)/EML (15 nm)/TmPyPB (35 nm)/LiF (1 nm)/Al (100 nm) for various colors, including blue, green, yellow, red, and white emission. MoO₃ and LiF serve as the hole injection layer and electron injection layer, respectively; TAPC is used as the hole-transporting layer (HTL); mCP is used as the second HTL and the exciton blocking layer; and TmPyPB serves as the electron-transporting layer and the hole-blocking layer. The energy level diagrams and molecular structures of the materials used in these devices are depicted in Fig. 5. The key device data are summarized in Table 2.

Considering the relatively low E_T at 2.44 eV, green and red PhOLEDs based on **TPA-BN** were fabricated employing common phosphorescent emitters Ir(ppy)₂(acac) and Ir(MDQ)₂(acac), respectively. Fig. 6 shows the current density–voltage–luminance (J – V – L), the power efficiency and EQE versus luminance characteristics, and the EL spectra of the two PhOLEDs. The relatively low turn-on voltages (V_{on} , at a luminance of 1 cd m⁻²) of 2.8 and 3.0 V for green and red PhOLEDs, respectively, were achieved because of the excellent matching of the energy levels of **TPA-BN** with those of the carrier transporting materials. The EL spectra of the green and red PhOLEDs in the inset of Fig. 6b are the typical emission of

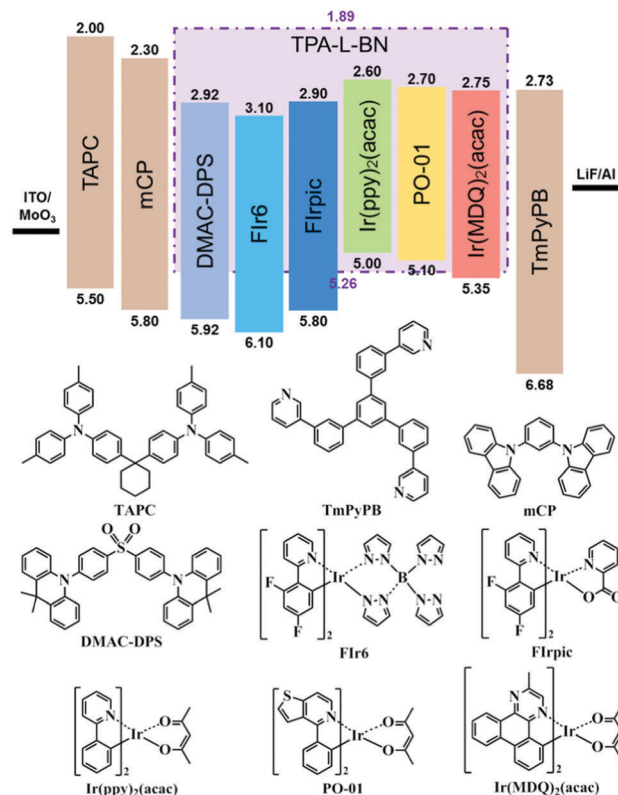


Fig. 5 Schematic energy level diagram and the molecular structures of the used materials, including 1,1-bis(di-4-tolylamino)phenyl)cyclohexane (TAPC), 1,3-bis(carbazol-9-yl)benzene (mCP), bis[4-(9,9-dimethyl-9,10-dihydroacridine)phenyl]sulfone (DMAC-DPS), iridium(III) bis(4',6'-difluorophenyl)pyridinato)tetrakis(1-pyrazolyl)borate (FIr6), iridium(III) bis(4,6-(difluorophenyl)pyridinato-*N,C*^{2'})picolinate (FIrpic), iridium(III) bis(2-phenylpyridinato-*N,C*^{2'})acetylacetonate (Ir(ppy)₂(acac)), iridium(III) bis(4-phenylthieno[3,2-*c*]pyridinato-*N,C*^{2'})acetylacetonate (PO-01), iridium(III) bis(2-methyldibenzo[*f,h*]quinoxaline)acetylacetonate (Ir(MDQ)₂(acac)), and 1,3,5-tri(*m*-pyrid-3-yl)phenyl)benzene (TmPyPB).

Ir(ppy)₂(acac) and Ir(MDQ)₂(acac) with Commission Internationale de L'Eclairage (CIE) coordinates of (0.321, 0.629) and (0.611, 0.387), indicating the effective energy transfer from **TPA-BN** to the emitters. The maximum EQE values of 20.3% and 21.4% were achieved by the green and red PhOLEDs, respectively, accompanied by the maximum power efficiencies (PEs) of 69.2 and 38.0 lm W⁻¹. In addition, the EQE values remained over 19% for both devices at a high luminance of 1000 cd m⁻² (Table 2), suggesting a low efficiency roll-off. These results indicate that **TPA-BN** can be good candidate for hosting green to red OLEDs.

The high E_T of 2.95 eV of **TPA-L-BN** indicates its ability to serve as host for deep blue to red emitters. To confirm this, first, the phosphorescent deep blue emitter FIr6, blue emitter FIrpic, and blue TADF emitter DMAC-DPS were chosen as dopants to fabricate blue phosphorescent and TADF devices. As shown in Fig. 7a and Table 2, the three devices have the same turn-on voltage of 3.2 V. However, the two blue PhOLEDs exhibited different J – V characteristics, probably due to the different emission mechanisms of the two phosphorescent emitters. At a doping concentration of 10 wt%, FIr6 has been proved to be able to

Table 2 Summary of the EL data of the phosphorescent and TADF OLEDs

EML ^a	Host	Guest	V_{on} ^b (V)	EQE (%)		CE_{max} ^e (cd A ⁻¹)	PE_{max} ^f (lm W ⁻¹)	CIE ^g (x, y)
				Max. ^c	@1000 ^d			
TPA-BN		Ir(ppy) ₂ (acac)	2.8	20.3	19.0	76.6	69.2	(0.321, 0.629)
TPA-BN		Ir(MDQ) ₂ (acac)	3.0	21.4	19.1	37.9	38.0	(0.611, 0.387)
TPA-L-BN		FIr6	3.2	18.3	15.9	39.3	33.5	(0.170, 0.285)
TPA-L-BN		FIrpic	3.2	19.8	15.6	43.9	38.2	(0.161, 0.320)
TPA-L-BN		DMAC-DPS	3.2	19.3	17.5	34.9	27.3	(0.163, 0.221)
TPA-L-BN		Ir(ppy) ₂ (acac)	2.8	20.0	19.4	76.2	70.5	(0.314, 0.637)
TPA-L-BN		PO-01	3.0	20.4	18.1	70.4	72.1	(0.475, 0.522)
TPA-L-BN		Ir(MDQ) ₂ (acac)	3.0	20.5	18.7	36.2	31.4	(0.612, 0.387)
TPA-L-BN		FIrpic, PO-01	3.0	21.7	19.5	62.8	57.8	(0.335, 0.432)/57 ^h
TPA-L-BN		DMAC-DPS, PO-01	3.0	21.1	18.7	53.8	48.8	(0.291, 0.345)/63 ^h
TPA-L-BN		FIrpic, Ir(ppy) ₂ (acac), Ir(MDQ) ₂ (acac)	3.0	23.4	20.5	57.1	53.6	(0.380, 0.440)/83 ^h

^a The uniform device structure: ITO/MoO₃ (5 nm)/TAPC (60 nm)/mCP (10 nm)/EML (15 nm)/TmPyPB (35 nm)/LiF (1 nm)/Al (100 nm). Doping concentrations are fixed at 10 wt% for monochrome OLEDs and 15 wt% PO-01 for complementary color WOLEDs. The EML of the three primary color WOLED is TPA-L-BN: 8 wt% Ir(MDQ)₂(acac) (8 nm)/TPA-L-BN: 5 wt% Ir(ppy)₂(acac) (3 nm)/TPA-L-BN: 15 wt% FIrpic (4 nm). ^b The applied voltage required for 1 cd m⁻². ^c Maximum external quantum efficiency (EQE). ^d EQE at 1000 cd m⁻². ^e Maximum current efficiency (CE). ^f Maximum power efficiency (PE). ^g EL recorded at 8 V. ^h Color rendering index (CRI) of the EL spectra at 8 V for WOLEDs.

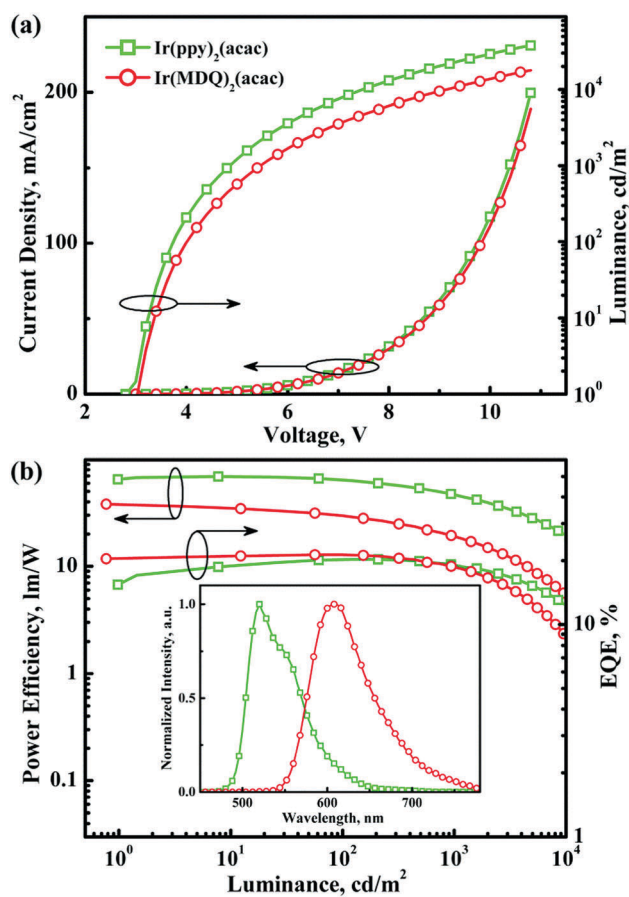


Fig. 6 (a) Current density–voltage–luminance (J – V – L) characteristics, (b) power efficiency and EQE as a function of luminance, and the normalized EL spectra (inset) of the green and red PhOLEDs based on TPA-BN.

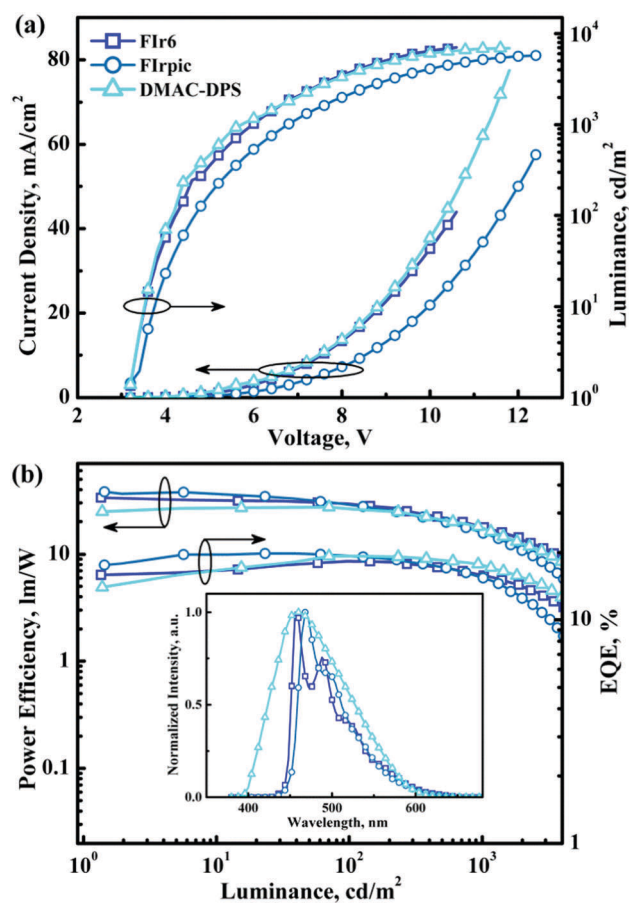


Fig. 7 (a) J – V – L characteristics, (b) power efficiency and EQE as a function of luminance, and normalized EL spectra (inset) of the blue phosphorescent and TADF OLEDs based on TPA-L-BN.

transport charge efficiently,⁵⁸ while the primary emission mechanism of FIrpic has been demonstrated to be the energy transfer process because of the independent J – V characteristics on FIrpic concentrations.⁵⁹ The maximum EQE values of 18.3% and 19.8% for the deep blue and blue PhOLEDs, respectively, demonstrate the

ability of TPA-L-BN to host deep blue and blue phosphorescent emitters. The maximum PEs of the two devices reached 33.5 lm W⁻¹ for FIr6 and 38.2 lm W⁻¹ for FIrpic, respectively, as shown in Fig. 7b. The blue TADF device also revealed a high maximum EQE of 19.3%, a current efficiency (CE) of 34.9 cd A⁻¹,

and a PE of 27.3 lm W^{-1} . The EL spectra of the three blue OLEDs are depicted in the inset of Fig. 7b. Inspired by the excellent performance of the **TPA-L-BN** based blue OLEDs, a series of PhOLEDs were fabricated with $\text{Ir}(\text{ppy})_2(\text{acac})$, PO-01, and $\text{Ir}(\text{MDQ})_2(\text{acac})$ as the green, orange, and red dopants, respectively. The J - V - L characteristics, PE and EQE curves, and EL spectra of these devices are shown in Fig. S3 (ESI[†]). It can be seen that low turn-on voltages of 2.8 to 3.0 V, high maximum EQE values over 20%, and EQEs higher than 18% at a luminance of 1000 cd m^{-2} were achieved in these three **TPA-L-BN** hosted PhOLEDs. The excellent performances of these devices substantially demonstrate the unique universal feature of **TPA-L-BN** as a host for both phosphorescent and TADF emitters.

To further verify the universality of **TPA-L-BN** as a host, a series of single-host WOLEDs were fabricated with the same abovementioned device structure where the EML was carefully designed to obtain stable white emission. The white EMLs usually employ emissive materials emitting two complementary colors (blue and orange) or three primary colors (blue, green, and red), to sufficiently cover the whole visible spectrum. Due to the simple structure and low fabrication cost, much attention has been paid to the single-EML structures in phosphorescent WOLEDs. Here, **TPA-L-BN** was first employed to fabricate the fully phosphorescent single-EML WOLED (device W1) where Flrpic and PO-01 were selected as complementary emitters with doping concentrations of 15 wt% and 1 wt%, respectively. As expected, device W1 showed excellent EL performance with a maximum CE of 62.8 cd A^{-1} , a maximum PE of 57.8, and a maximum EQE of 21.7%. The EQE value was slightly reduced to 19.5% at a luminance of 1000 cd m^{-2} , as displayed in Fig. 8 and Table 2.

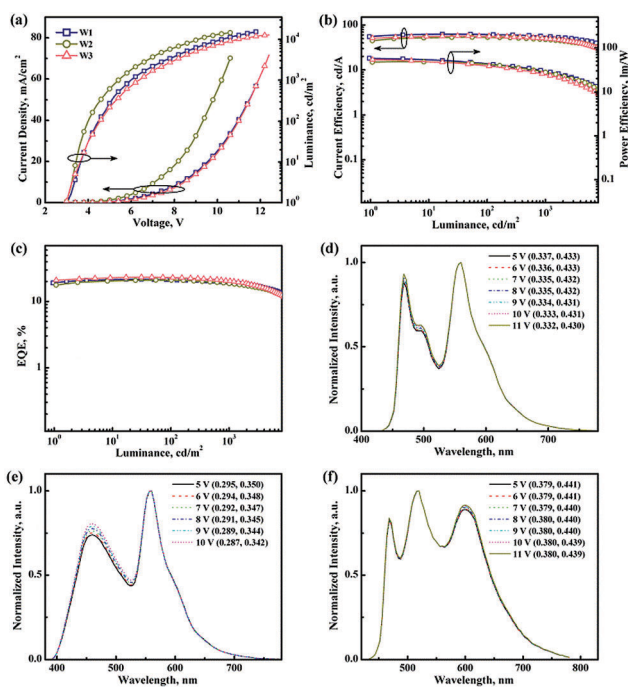


Fig. 8 (a) J - V - L characteristics, (b) current efficiency and power efficiency as a function of luminance, (c) EQE as a function of luminance, and normalized EL spectra of devices W1 (d), W2 (e), and W3 (f).

In Fig. 8d, the EL spectrum showed a balanced blue and orange emission with the intrinsic emission from both Flrpic and PO-01 with CIE coordinates of (0.335, 0.432) at 8 V. When the voltage increased from 5 to 11 V, a small CIE coordinate variation of (0.005, 0.003) demonstrated the good color stability of device W1. The high efficiencies, low efficiency roll-off, and stable chromaticity of device W1 can be attributed to the high E_T value and bipolar feature of **TPA-L-BN**, and the precise manipulation of charges and excitons through the device structure and doping strategy in EMLs.⁶⁰ Encouraged by the satisfactory performance of device W1, the TADF/phosphorescent hybrid single-EML WOLED (device W2) was prepared by using the blue TADF emitter DMAC-DPS combined with the orange phosphorescent emitter PO-01 as complementary emitters. Maximum CE, PE, and EQE values of 53.8 cd A^{-1} , 48.8 lm W^{-1} , and 21.1% were obtained with stable cool white emission (Fig. 8 and Table 2). It is noteworthy that the color rendering index (CRI) values of 57 and 63 for W1 and W2, respectively, are relatively low because of the two complementary color systems. To improve the CRI, the single-host three primary color WOLED (device W3) was fabricated where the EML was optimized as **TPA-L-BN**: $\text{Ir}(\text{MDQ})_2(\text{acac})$ (8 wt%, 8 nm)/**TPA-L-BN**: $\text{Ir}(\text{ppy})_2(\text{acac})$ (5 wt%, 3 nm)/**TPA-L-BN**: Flrpic (15 wt%, 4 nm).¹¹ The impressive performance of device W3 was also achieved with a peak EQE of 23.4% and a slight decline to 20.5% at 1000 cd m^{-2} . The CIE coordinates varied very slightly from (0.379, 0.441) at 5 V to (0.380, 0.439) at 11 V, demonstrating high color stability (Fig. 8f). Furthermore, the spectrum of device W3 showed a rather high CRI maintained at 83 across the whole range of luminance. Overall, effective carrier/exciton confinement, balanced charge carriers, broad and stable distribution of the recombination region, and optimization of the EML for efficient energy transfer give rise to these excellent device results for **TPA-L-BN** based WOLEDs.

Besides high efficiency, a long operational lifetime is also essential for the OLED technology to achieve practical applications. Bipolar hybrids with a flexible linkage have the potential for strengthening the morphological stability of a glassy EML against phase separation and crystallization.^{40,41,43,61} As shown in Fig. 9, thermal annealing of amorphous neat films and doped films with $\text{Ir}(\text{ppy})_2(\text{acac})$ of **TPA-BN** and **TPA-L-BN** exhibited widely varying morphological stability. After thermal annealing at 40°C for 48 h, both **TPA-L-BN** films remained amorphous, while the polycrystalline nature was observed by polarizing optical microscopy with both the neat film and doped film of **TPA-BN**. The morphological stability of the **TPA-L-BN** films should contribute at least in part to the longevity of the corresponding OLEDs. To confirm this, the lifetime of the green PhOLEDs was evaluated with the device structure of ITO/MoO_3 (5 nm)/NPB (80 nm)/**TPA-BN** or **TPA-L-BN**: $\text{Ir}(\text{ppy})_2(\text{acac})$ (8 wt%, 15 nm)/BCP (10 nm)/ Alq_3 (30 nm)/LiF (1 nm)/Al (100 nm). Fig. 9e shows the lifetime curves of the green PhOLEDs measured at an initial luminance of 3000 cd m^{-2} . The device hosted by **TPA-L-BN** showed a much longer lifetime than that of the device using **TPA-BN** as a host, indicating the crucial role of the flexible spacer to maintain the morphological stability of the host materials in the solid state and render a longer lifetime of the device.

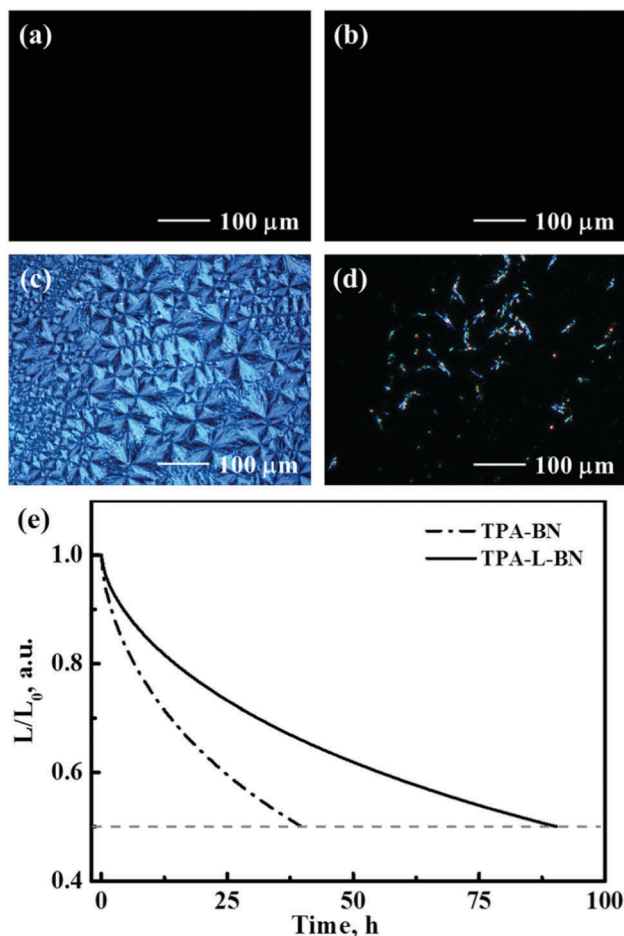


Fig. 9 Polarizing optical micrographs of spin-cast films of (a) TPA-L-BN, (b) TPA-L-BN: 8 wt% Ir(ppy)₂(acac), (c) TPA-BN, and (d) TPA-BN: 8 wt% Ir(ppy)₂(acac) under thermal annealing at 40 °C for 48 h, and (e) normalized luminance of as a function of operating time for the green PhOLEDs using the two hosts.

Conclusions

In summary, two representative hybrid compounds with distinct chemical linkages, TPA-BN and TPA-L-BN, were synthesized to evaluate their potential as hosts for both phosphorescent and TADF OLEDs. The systematical characterization of their thermal, morphological, electrochemical, photophysical, charge transporting, and electroluminescent properties revealed that the non-conjugated hybrid TPA-L-BN with a flexible aliphatic spacer could serve as a universal host material for highly efficient and stable phosphorescent and TADF OLEDs. With a high E_T value, suitable frontier molecular orbital levels, bipolar charge carrier transporting capability, and excellent morphological stability, TPA-L-BN was utilized for hosting deep blue to red emitters in a simple and unified device structure. The monochrome phosphorescent and TADF OLEDs hosted by TPA-L-BN revealed high efficiencies and low roll-offs with various colors from DMAC-DPS, FIr6, FIrpic, Ir(ppy)₂(acac), PO-01, and Ir(MDQ)₂(acac). In addition, the single-host WOLEDs achieved both high efficiencies and stable white emission by adopting not only all phosphorescent

but also TADF/phosphorescent hybrid EMLs. The three primary color WOLED showed an improved CRI of 83 which was independent of the driving voltage in the range of 5 to 11 V. Moreover, the operational lifetime of the TPA-L-BN hosted device was considerably enhanced compared to that of the device based on TPA-BN. Altogether, the introduction of the flexible linkage has been demonstrated to be an effective approach to construct universal host materials for highly efficient and stable phosphorescent and TADF OLEDs.

Conflicts of interest

There are no conflicts to declare.

Acknowledgements

We acknowledge the financial support from the National Key Research and Development Program of China (No. 2016YFB0401005) funded by MOST, the Program for Science and Technology Innovation Team of Shaanxi Province (2018TD-030), the Natural Science Basic Research Plan in Shaanxi Province of China (2017JM5058), the Funded Projects for the Academic Leaders and Academic Backbones, Shaanxi Normal University (16QNGG008), and the Fundamental Research Funds for the Central Universities (GK201802014).

References

- 1 C. W. Tang and S. A. VanSlyke, *Appl. Phys. Lett.*, 1987, **51**, 913–915.
- 2 T. W. Kelley, P. F. Baude, C. Gerlach, D. E. Ender, D. Muyres, M. A. Haase, D. E. Vogel and S. D. Theiss, *Chem. Mater.*, 2004, **16**, 4413–4422.
- 3 N. Thejo Kalyani and S. J. Dhoble, *Renewable Sustainable Energy Rev.*, 2012, **16**, 2696–2723.
- 4 H. Sasabe and J. Kido, *J. Mater. Chem. C*, 2013, **1**, 1699–1707.
- 5 M. A. Baldo, D. F. O'Brien, Y. You, A. Shoustikov, S. Sibley, M. E. Thompson and S. R. Forrest, *Nature*, 1998, **395**, 151–154.
- 6 H. Uoyama, K. Goushi, K. Shizu, H. Nomura and C. Adachi, *Nature*, 2012, **492**, 234–238.
- 7 Q. Wang and D. G. Ma, *Chem. Soc. Rev.*, 2010, **39**, 2387–2398.
- 8 K. T. Kamtekar, A. P. Monkman and M. R. Bryce, *Adv. Mater.*, 2010, **22**, 572–582.
- 9 Z. Wu and D. Ma, *Mater. Sci. Eng., R*, 2016, **107**, 1–42.
- 10 F. Zhao and D. Ma, *Mater. Chem. Front.*, 2017, **1**, 1933–1950.
- 11 Q. Wang, J. Ding, D. Ma, Y. Cheng, L. Wang and F. Wang, *Adv. Mater.*, 2009, **21**, 2397–2401.
- 12 S. Gong, Y. Chen, C. Yang, C. Zhong, J. Qin and D. Ma, *Adv. Mater.*, 2010, **22**, 5370–5373.
- 13 B. Zhang, G. Tan, C. S. Lam, B. Yao, C. L. Ho, L. Liu, Z. Xie, W. Y. Wong, J. Ding and L. Wang, *Adv. Mater.*, 2012, **24**, 1873–1877.
- 14 C. J. Zheng, J. Wang, J. Ye, M. F. Lo, X. K. Liu, M. K. Fung, X. H. Zhang and C. S. Lee, *Adv. Mater.*, 2013, **25**, 2205–2211.

- 15 Y. Sun, N. C. Giebink, H. Kanno, B. Ma, M. E. Thompson and S. R. Forrest, *Nature*, 2006, **440**, 908–912.
- 16 G. Schwartz, M. Pfeiffer, S. Reineke, K. Walzer and K. Leo, *Adv. Mater.*, 2007, **19**, 3672–3676.
- 17 Y. Chen, F. Zhao, Y. Zhao, J. Chen and D. Ma, *Org. Electron.*, 2012, **13**, 2807–2815.
- 18 N. Sun, Q. Wang, Y. Zhao, Y. Chen, D. Yang, F. Zhao, J. Chen and D. Ma, *Adv. Mater.*, 2014, **26**, 1617–1621.
- 19 Y. Li, Z. Wang, X. Li, G. Xie, D. Chen, Y.-F. Wang, C.-C. Lo, A. Lien, J. Peng, Y. Cao and S.-J. Su, *Chem. Mater.*, 2015, **27**, 1100–1109.
- 20 F. Zhao, Y. Wei, H. Xu, D. Chen, T. Ahamad, S. Alshehri, Q. Pei and D. Ma, *Mater. Horiz.*, 2017, **4**, 641–648.
- 21 Q. Sun, Y. Hu, Y. Dai and D. Ma, *J. Mater. Chem. C*, 2017, **5**, 8022–8026.
- 22 C. Shi, N. Sun, Z. Wu, J. Chen and D. Ma, *J. Mater. Chem. C*, 2018, **6**, 767–772.
- 23 D. Zhang, L. Duan, Y. Zhang, M. Cai, D. Zhang and Y. Qiu, *Light: Sci. Appl.*, 2015, **4**, e232.
- 24 D. Zhang, M. Cai, Y. Zhang, D. Zhang and L. Duan, *ACS Appl. Mater. Interfaces*, 2015, **7**, 28693–28700.
- 25 Z. Wu, J. Luo, N. Sun, L. Zhu, H. Sun, L. Yu, D. Yang, X. Qiao, J. Chen, C. Yang and D. Ma, *Adv. Funct. Mater.*, 2016, **26**, 3306–3313.
- 26 J. Y. Wu and S. A. Chen, *ACS Appl. Mater. Interfaces*, 2018, **10**, 4851–4859.
- 27 J. Liang, C. Li, X. Zhuang, K. Ye, Y. Liu and Y. Wang, *Adv. Funct. Mater.*, 2018, **28**, 1707002.
- 28 Y. J. Cho, K. S. Yook and J. Y. Lee, *Adv. Mater.*, 2014, **26**, 4050–4055.
- 29 L. S. Cui, Y. M. Xie, Y. K. Wang, C. Zhong, Y. L. Deng, X. Y. Liu, Z. Q. Jiang and L. S. Liao, *Adv. Mater.*, 2015, **27**, 4213–4217.
- 30 K. Gao, K. Liu, X.-L. Li, X. Cai, D. Chen, Z. Xu, Z. He, B. Li, Z. Qiao, D. Chen, Y. Cao and S.-J. Su, *J. Mater. Chem. C*, 2017, **5**, 10406–10416.
- 31 Y. Zhao, C. Wu, P. Qiu, X. Li, Q. Wang, J. Chen and D. Ma, *ACS Appl. Mater. Interfaces*, 2016, **8**, 2635–2643.
- 32 Y. Tao, C. Yang and J. Qin, *Chem. Soc. Rev.*, 2011, **40**, 2943–2970.
- 33 L. Xiao, Z. Chen, B. Qu, J. Luo, S. Kong, Q. Gong and J. Kido, *Adv. Mater.*, 2011, **23**, 926–952.
- 34 L. Duan, J. Qiao, Y. Sun and Y. Qiu, *Adv. Mater.*, 2011, **23**, 1137–1144.
- 35 A. Chaskar, H. F. Chen and K. T. Wong, *Adv. Mater.*, 2011, **23**, 3876–3895.
- 36 K. S. Yook and J. Y. Lee, *Chem. Rec.*, 2016, **16**, 159–172.
- 37 G. Horowitz and M. E. Hajlaoui, *Adv. Mater.*, 2000, **12**, 1046–1050.
- 38 T. Yamada, T. Hasegawa, M. Hiraoka, H. Matsui, Y. Tokura and G. Saito, *Appl. Phys. Lett.*, 2008, **92**, 233306.
- 39 F. So and D. Kondakov, *Adv. Mater.*, 2010, **22**, 3762–3777.
- 40 L. Zeng, T. Y.-H. Lee, P. B. Merkel and S. H. Chen, *J. Mater. Chem.*, 2009, **19**, 8772–8781.
- 41 Q. Wang, J. U. Wallace, T. Y.-H. Lee, J. J. Ou, Y.-T. Tsai, Y.-H. Huang, C.-C. Wu, L. J. Rothberg and S. H. Chen, *J. Mater. Chem. C*, 2013, **1**, 2224–2232.
- 42 Q. Wang, J. U. Wallace, T. Y.-H. Lee, L. Zeng, J. J. Ou and S. H. Chen, *Org. Electron.*, 2013, **14**, 2925–2931.
- 43 Q. Wang, Z. Wu, Y. Zhao, J. Chen and D. Ma, *Org. Electron.*, 2016, **32**, 21–26.
- 44 C. Wu, Q. Guo, W. Ma, X. Li, P. Qiu, J. Hu, Q. Wang, J. Chen and D. Ma, *Phys. Chem. Chem. Phys.*, 2017, **19**, 5177–5184.
- 45 S. Tao, L. Li, J. Yu, Y. Jiang, D. Zhou, C.-S. Lee, S.-T. Lee, X. Zhang and O. Kwon, *Chem. Mater.*, 2009, **21**, 1284–1287.
- 46 E. Polikarpov, J. S. Swensen, N. Chopra, F. So and A. B. Padmaperuma, *Appl. Phys. Lett.*, 2009, **94**, 223304.
- 47 F.-M. Hsu, C.-H. Chien, C.-F. Shu, C.-H. Lai, C.-C. Hsieh, K.-W. Wang and P.-T. Chou, *Adv. Funct. Mater.*, 2009, **19**, 2834–2843.
- 48 Y. Tao, K. Yuan, T. Chen, P. Xu, H. Li, R. Chen, C. Zheng, L. Zhang and W. Huang, *Adv. Mater.*, 2014, **26**, 7931–7958.
- 49 M. Godumala, S. Choi, M. J. Cho and D. H. Choi, *J. Mater. Chem. C*, 2016, **4**, 11355–11381.
- 50 M. Y. Wong and E. Zysman-Colman, *Adv. Mater.*, 2017, **29**, 1605444.
- 51 Z. Yang, Z. Mao, Z. Xie, Y. Zhang, S. Liu, J. Zhao, J. Xu, Z. Chi and M. P. Aldred, *Chem. Soc. Rev.*, 2017, **46**, 915–1016.
- 52 Y. Tao, Q. Wang, C. Yang, C. Zhong, J. Qin and D. Ma, *Adv. Funct. Mater.*, 2010, **20**, 2923–2929.
- 53 C. Wu, Z. Wu, B. Wang, X. Li, N. Zhao, J. Hu, D. Ma and Q. Wang, *ACS Appl. Mater. Interfaces*, 2017, **9**, 32946–32956.
- 54 Y. Tao, Q. Wang, L. Ao, C. Zhong, J. Qin, C. Yang and D. Ma, *J. Mater. Chem.*, 2010, **20**, 1759–1765.
- 55 G. Malleshham, C. Swetha, S. Niveditha, M. E. Mohanty, N. J. Babu, A. Kumar, K. Bhanuprakash and V. J. Rao, *J. Mater. Chem. C*, 2015, **3**, 1208–1224.
- 56 J. Pommerehne, H. Vestweber, W. Guss, R. F. Mahrt, H. Bässler, M. Porsh and J. Daub, *Adv. Mater.*, 1995, **7**, 551–554.
- 57 A. Degli Esposti, V. Fattori, C. Sabatini, G. Casalbore-Miceli and G. Marconi, *Phys. Chem. Chem. Phys.*, 2005, **7**, 3738–3743.
- 58 R. J. Holmes, B. W. D'Andrade, S. R. Forrest, X. Ren, J. Li and M. E. Thompson, *Appl. Phys. Lett.*, 2003, **83**, 3818–3820.
- 59 Q. Wang, J. Ding, D. Ma, Y. Cheng and L. Wang, *Appl. Phys. Lett.*, 2009, **94**, 103503.
- 60 Q. Wang, J. Ding, D. Ma, Y. Cheng, L. Wang, X. Jing and F. Wang, *Adv. Funct. Mater.*, 2009, **19**, 84–95.
- 61 T. Y.-H. Lee, Q. Wang, J. U. Wallace and S. H. Chen, *J. Mater. Chem.*, 2012, **22**, 23175–23180.